Grading evolution of an artificial granular material from medium to high stress under one-dimensional compression

by Francesca Casini*, Giulia Guida†, Manuel Bartoli*, Giulia M.B. Viggiani*

* Università di Roma Tor Vergata

† Università Niccolò Cusano

Contact Author:

Prof. Francesca Casini

Dipartimento di Ingegneria Civile

Università di Roma Tor Vergata

Via del Politecnico, 1

00133 Roma ITALY

ph.: +39 0672597051

fax: +39 0672597005

e-mail: francesca.casini@uniroma2.it

Keywords:

Grain crushing, Grain size distribution, Weibull function, Compressibility

Abstract

This contribution presents the results of an experimental investigation of the mechanical behaviour of granular materials with crushable grains under one-dimensional compression at medium to high stress. The material used for the experimental work is a Light Expanded Clay Aggregate (LECA) whose grains break at relatively low stress. Reconstituted samples were prepared with different initial grain size distributions and their evolution observed under one-dimensional compression. The grain size distributions before and after testing were used to calibrate a bimodal model obtained from the superposition of two Weibull functions. The observed evolution of the micro and macro diameters on loading are linked to the characteristics of the one-dimensional compressibility curve obtained under displacement controlled conditions, such as its shape and two characteristic stress values, namely the pre-consolidation stress and the stress corresponding to the point of inflection.

Introduction

Loading induced particle breakage has important effects on the mechanical behaviour and hydraulic conductivity of granular materials. Particle breakage has been observed from the relatively small scale of laboratory samples (*e.g.*, Nakata *et al.,* 2001; Casini *et al.,* 2013; Bandini *et al.,* 2016; Ziccarelli 2016) to the very large scale of real faults exhumed from seismogenic depths (Sammis & Ben-Zion, 2008). Grain crushing controls many engineering applications characterised by high stress concentration, such as near the tip of piles, with effects on their bearing capacity (see, *e.g.*, Yasufuhu & Hide, 1995; Simonini, 1996; Lobo-Guerrero & Vallejo, 2005; Zhang *et al*., 2012) or in highly stressed soil masses adjacent to or located within geotechnical structures, for instance filters for large dams (Lee & Farhoomand, 1967) or rockfill dams (Alonso *et al.,* 2012; Ovalle *et al.,* 2014). Okada *et al*. (2004) reported that grain crushing within the failure zone is responsible for the rapid long run-out of landslides, while, more recently, Marks & Einav (2015) examined the interplay between grain crushing and segregation, controlling the dynamics of dense granular flows.

Whatever the engineering application, to identify the main factors controlling grain crushing, the evolution of the grain size distribution upon loading must be examined experimentally over a wide range of stress. The evolution of grading with loading depends on various factors at different scales. At the macro scale, crushing is controlled by initial grading, voids ratio, state of effective stress, and effective stress path; at the meso - micro scale, by the parameters of the constituent particles, such as, *e.g.*, size, shape, strength, and mineral composition.

The available experimental evidence (*e.g*. Hardin, 1985; Casini *et al.,* 2013; Guida *et al.,* 2016) indicates that well-graded soils do not break down as easily as uniform soils and that, as the relative density increases, the amount of particle breakage decreases. Both these observations are consistent with the fact that, with more particles surrounding each particle, the average contact stress tends to decrease. Several researchers have found that the amount of grain crushing under isotropic loading conditions is lower than under shearing (Nakata et *al*., 1999, Luzzani & Coop, 2002; Lackenby *et al*., 2007). As far as the characteristics of the constituent particles are concerned, it is well established that (Lade, 1996): as the particle size increases, particle crushing increases, due to the fact that larger particles have a higher probability of containing defects or flaws; increasing the particle angularity increases particle breakage; increasing the mineral hardness decreases the amount of particle crushing.

The amount of breakage induced by loading has been quantified in different ways (*e*.g. Hardin, 1985; Einav, 2007; Wood & Maeda, 2008) based on the relative position of the current and initial cumulative grain size distributions. Hardin (1985) introduced relative breakage, B_r based on the area between the final and initial grain size distributions above an arbitrary cut-off value of 'silt' particle size (of 0.074 mm). This implies that, in the fragmentation process, all particles, no matter what their original size is, will eventually become finer than this arbitrary cut-off value. Einav (2007) proposed to adjust the original definition of the relative breakage by Hardin (1985) to weigh from zero to one the relative proximity of the current grain size cumulative distribution from an initial cumulative distribution, and an ultimate cumulative distribution. Wood & Maeda (2008) proposed to use a single reference initial cumulative distribution as a vertical line through the maximum diameter, with the implication that the initial grading of any sample corresponds to a non-zero initial value of B_r.

As pointed out by Wood and Maeda (2008), in order to be able to predict the effects of a change in the grain size distribution there are three requirements: (i) the definition of some grading state index which can be used to describe the current grading of the soil; (ii) an evolution law which describes the way in which this grading state index changes with the state of stress; (iii) and some rules which describe the influence that the changing grading state index has on the mechanical properties of the soil. Casini *et al.* (2013) discussed the second of these requirements based on a wide set of experimental data on grading evolution of an artificial granular material, that break at relatively low stress. The grading evolution of the material after isotropic, one-dimensional and constant mean effective stress triaxial compression were studied with the mean effective stress ranging between 0.175 and 1.400 MPa on samples reconstituted with different values of U (= d_{60}/d_{10}) = 3.5, 7, 14, and 28 and two mean values of mean grain size $d_{50} = 0.5$ and 1 mm. The Authors linked the evolution of relative breakage, B_r, defined following the approach proposed by Wood & Maeda (2008), with the total work input for unit of volume. They concluded that, for poorly graded samples (up to $U = 14$), the rate of breakage is independent of the initial uniformity while, for well-graded samples ($U = 28$), the maximum rate of breakage is smaller and particle breakage results in a progressive increase of the fines and a reduction of the maximum diameter.

In this work, the same granular material used by Casini *et al.* (2013) was tested in one-dimensional compression over a wide range of stress, $\sigma_{v,max}$ = 0.25 to 50.00 MPa. The grain size distributions before and after loading were described using a bimodal Weibull distribution calibrated using the experimental data.

Grain crushing upon loading produces a progressive clockwise rotation of the cumulative grain size distribution around the point corresponding to the maximum diameter, with a tendency of the percentage of finer particles to increase and limited reduction of the maximum diameter. The paper examines the relationship between particle crushing and the observed S-shaped compressibility curve. Two characteristics stress, namely the yield stress, σ_p, and the stress corresponding to point of inflection of the compressibility curve, σ_s, mark the transition between different patterns of particle breakage.

1. Experimental work

1.1 Material

The degradation processes associated with grain crushing affect the natural behaviour of many natural geotechnical materials such as pyroclastic weak rocks, carbonate sands, calcarenites and residual soils. However, systematic experimental investigation of grain crushing for natural materials is often difficult due to the relatively high stress required to crush the grains and the variability and heterogeneity of natural deposits, which makes it difficult to obtain repeatable results. For these reasons, the experimental work discussed in this paper was carried out on an artificial granular material consisting of crushed expanded clay pellets, whose grains break at relatively low stress. The material, obtained machining a clay paste into pellets by means of a thermal process of clinkerization (Casini *et al.,* 2013; Guida *et al.,* 2016), is commercially available under the acronym LECA (Light Expanded Clay Aggregate). Due to its low unit weight, this material is used in many civil engineering applications to construct road embankments or slopes, create compensated foundations and as backfill of retaining structures. The advantages of using light materials may be in term of settlement reduction and improved seismic response (Di Prisco & Buscarnera, 2010). The grains have an external hard cortex and an internal extremely porous matrix. LECA pellets are commercially available in various sizes both intact and fragmented; while intact pellets are characterised by a round and isometric morphology, their fragments are extremely rough and irregular, partly because fragmentation exposes their internal porosity.

The material is characterised by a double order of porosity: "inter-granular", *i.e.* voids existing between particles, and "intra-granular", *i.e.* closed voids existing within individual particles. The apparent unit weight can be defined as $\gamma_{sa} = P_s/V_{sa}$, where P_s is the solid weight and $V_{sa} = V_s + V_{vi}$ is the apparent volume, with V_s volume of solid and V_{vi} volume of closed voids. The apparent unit weight γ_{sa} is related to the solid unit weight γ_s by the following equation: $\gamma_{sa}=\gamma_s/(1+e_i)$ where $e_i=V_{vi}/V_s$ is the intra granular void ratio (see Fig. 1).

The apparent unit weight, γ_{sa}, increases significantly with decreasing grain size for $d < 0.063$ mm and tends to the unit weight of the constituent clay ($\gamma_s = 26.5$ kN/m^3), while, for d larger than about 3.5 mm, it tends to a constant value of about 9 kN/m^3. For $d < 3.5$ mm, of interest in the present work, the experimental values of γ_{as} were fitted with the Equation (1).

$$\gamma_{sa}(d) = a\left(\frac{d}{d_0}\right)^{-b} \quad (1)$$

with $a = 12.64$ kN/m^3, $b = 0.268$, and $d_0 = 1$ mm, for $d \geq 0.063$ mm, and $\gamma_{as} = \gamma_s$, for $d < 0.063$ mm. Figure 1 shows also the trend of e_i versus d. The intra void ratio e_i increases with the particle diameter d assuming values larger than 1 for particles with $d \geq 0.84$ mm, with the implication that the intra void volume is larger than the solid volume of the particle; e_i decreases for decreasing d and is equal to zero for d < 0.06 mm where the apparent unit weight γ_{sa}=γ_s.

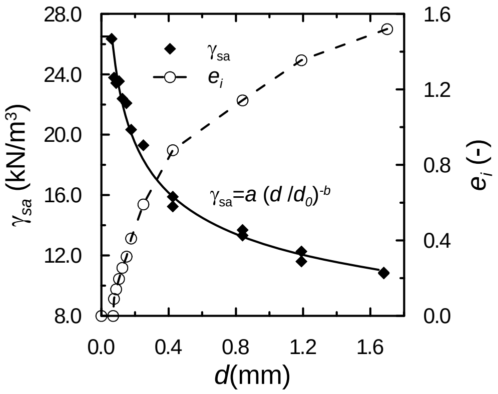

Figure 1. Apparent unit weight γ_{sa} of crushed LECA and intra void ratio e_i function of grain size.

1.2 Initial grain size distribution

The material was reconstituted at different initial grain size distributions by weight, characterised by four values of the coefficient of uniformity U (= d_{60}/d_{10}) = 3.5, 7, 14, and 28 and two values of mean grain size d_{50} = 0.5 mm and 1 mm (Figure 2a). For a material such as LECA, in which the apparent unit weight of particles depends on grain size, it is necessary to distinguish between the grain size distribution by weight and the grain size distribution by volume. The volume of particles retained in the i-th sieve is $V_i = W_i/\ \gamma_{sa,i}$, where Wi is the weight retained by the single sieve and $\gamma_{sa,i}$ is the average apparent unit weight of the particles in the size range $\Delta_{i\text{-}1} < d < \Delta_i$ with Δ_i is the dimension of the sieve (Equation (2)).

$$\gamma_{sa,i} = \frac{1}{\Delta_i - \Delta_{i-1}} \int_{\Delta_{i-1}}^{\Delta_i} \gamma_{sa}\,(d)\,\mathrm{d}d = \frac{a\left((\Delta_i)^{1-b} - (\Delta_{i-1})^{1-b}\right)}{(d_0)^b(\Delta_i - \Delta_{i-1})(1-b)} \qquad (2)$$

where $\gamma_{sa}(d)$ is given by Equation.(1).

The cumulative grain size distribution by volume can be computed as shown in Equation. (3):

$$V(d_j) = \frac{W(d<\Delta_1)/\gamma_{sa,1} + \sum_{i=2}^{j\leq N} V_i}{V_T} \qquad (3)$$

in which $\gamma_{sa,1}$ is the average unit weight of the material with dimensions smaller than Δ_1 and $V_T = W(d < \Delta_1)/\gamma_{sa,1} + \sum_{i=2}^{N} V_i$, is the total (apparent) volume of the solids in the sample (after Casini *et al.,* 2013)

Figures 2a-b show the initial grain size distributions by weight and by volume tested under 1D compression. The initial GSDs can be described with the fractal equation $P = (d/d_{max})^{\beta}$ where d_{max} is the maximum diameter and $\beta = 3-\alpha$ is the fractal dimension. The equation parameters can be computed as $d_{max} = d_{50}/0.5^{1/\beta}$ and $\beta = \log_U 6$. The corresponding values of parameters β_p (by weight) and β_v (by volume) of the tested initial GSDs are reported in Figure 2c as a function of the initial uniformity U. As U increases, the values of β decrease, reaching an asymptotic horizontal value for $U \geq 40$. In the range of interest ($U = 3.5$-28) β_p (by weight) assumes lower values than β_v (by volume). β represents the slope of GSDs curve, and the slope of the GSDs by weight is lower than the GSDs by volume because smaller diameters *d* have larger unit weight than bigger ones.

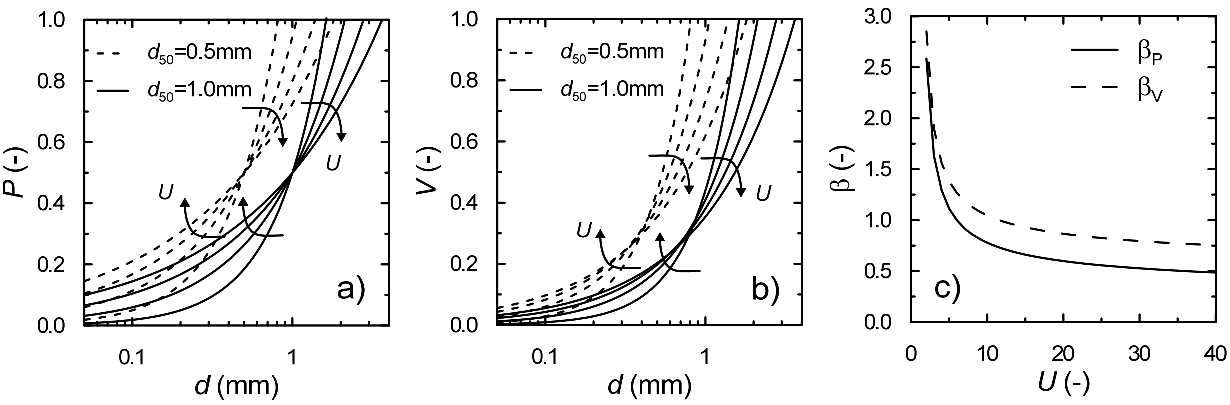

Figure 2. a) initial GSDs by weight; b) initial GSDs by volume for U=3.5,7.0,14,28 and d_{50}=0.5,1.0 mm; c) β versus uniformity coefficient U.

1.3 Evolution of grain size distribution with loading

The experimental programme consisted of 64 one-dimensional compression tests with a maximum vertical stress spanning from 0.25 MPa to 50 MPa (see Table 1). More in detail, three sets of 1-D compression tests were carried out, depending on the range of maximum vertical stress attained during the test: for $0.25 \leq \sigma_{v,max} \leq 2$ MPa, standard incremental loading oedometer tests on samples with diameter $D = 71.36$ mm and height $H = 20$ mm; for $5 \leq \sigma_{vmax} \leq 12.6$ MPa, displacement controlled 1D compression at a constant axial displacement rate of 1 mm/min, on samples with $D = 100$ mm and $H = 40$ mm, using a loading frame with maximum capacity of 100 kN, corresponding to a maximum vertical stress $\sigma_{v,max} = 12.6$ MPa; for $25 \leq \sigma_{v,max} \leq 50$ MPa, displacement controlled 1D compression at a constant axial displacement rate of 1 mm/min, on samples with $D = 50$ mm and $H = 80$ mm, using the same loading frame whose capacity in this case corresponds to a maximum vertical stress $\sigma_{vmax} = 50$ MPa. The dimensions of the samples for the last series of tests derives from a compromise between conflicting issues: reaching high level of stress, avoiding boundary effects and reducing lateral friction. For a given apparatus force capacity, an increasing vertical stress level is reachable reducing the diameter of the cell. Large values of stress $\sigma_{v,max}$, inducing huge axial displacements, reduce the distance between the plates so far to give rise to boundary effects on state of stress. To avoid this kind of boundary effect, for the high stress tests, a taller sample is adopted, which however led to an increase of lateral friction not considered in this study (Guida *et al.,* 2016). The procedure to reconstitute the samples consists of: (i) preparing the initial GSD by sieving, (ii) manual mixing, (iii) dry pluviation inside the cell.

Figure 3 shows the deformation measured at the target vertical stress as function of the samples initial uniformity for $d_{50} = 0.50$ mm (Fig. 3a) and $d_{50} = 1$ mm (Fig. 3b). For $U = 3.5$ and $d_{50} = 0.5$ mm (Fig. 3a), the vertical deformation increases with σ_{vmax} from a minimum of $\varepsilon_{amin} \sim 0.1$ with $\sigma_{vmax} = 0.25$ MPa, to a maximum of $\varepsilon_{amax} \sim 0.62$ at $\sigma_{vmax} = 50$ MPa. Similar trends were obtained for other values of U and for $d_{50} = 1.0$ mm. At low stress levels (up to 1-2 MPa), the values of final vertical deformation are independent of U while at higher stress (≥ 2.0 MPa), the better graded samples, with higher values of U, show a stiffer response. This may be attributed to a more effective cushioning effect, taking place for the better-graded samples, due to a better packing and an increases in the coordination number.

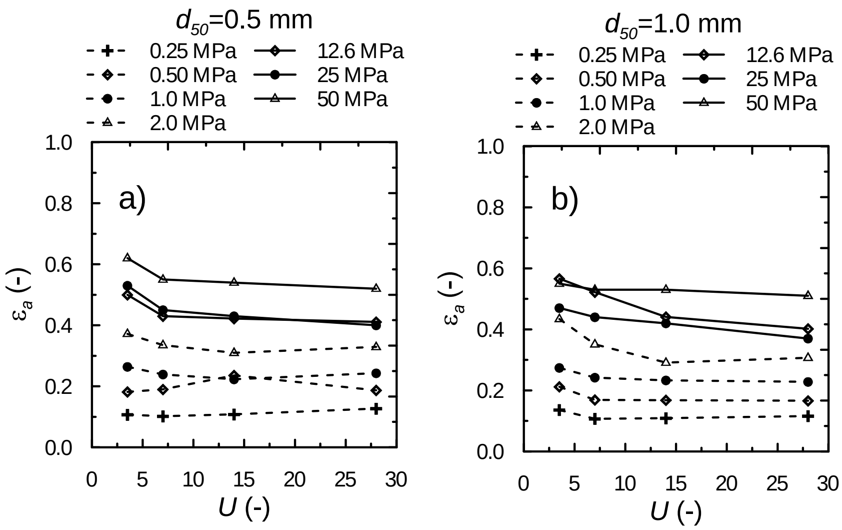

Figure 3. Maximum measured axial deformation, ε_a, versus initial uniformity, U: a) d_{50}=0.5 mm; b) d_{50}=1 mm.

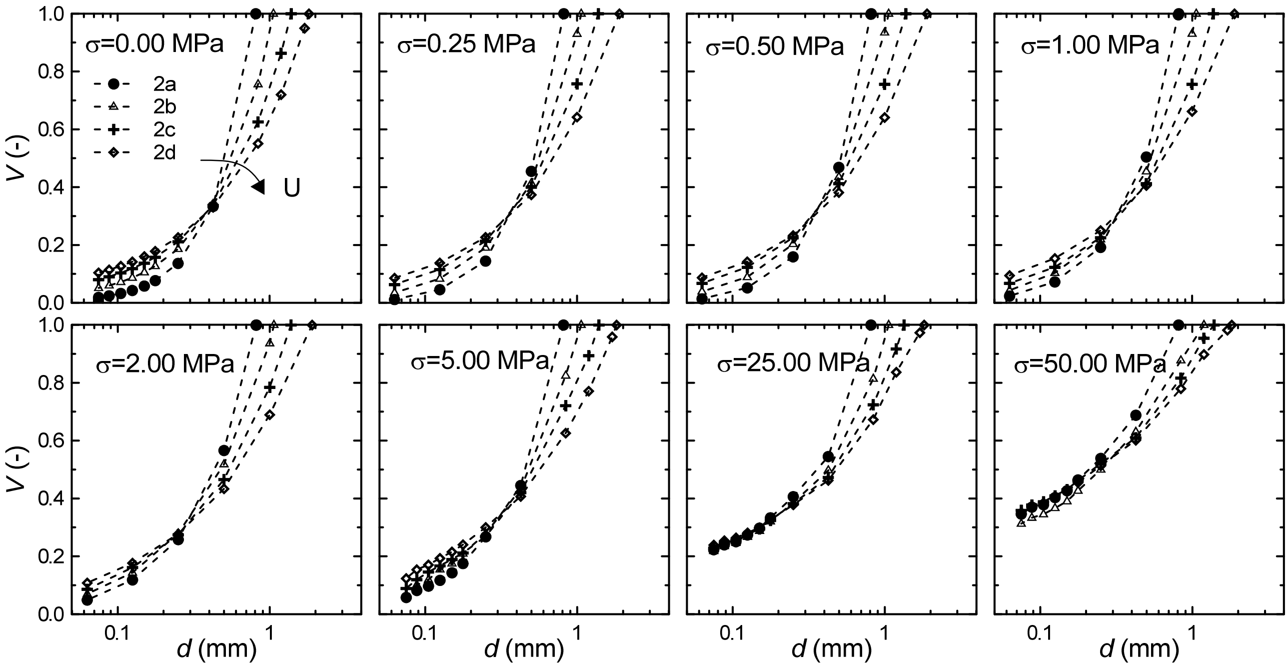

Figure 4. Grain size distribution by volume at increasing vertical stress for samples with with d_{50}=0.50 mm

Figure 4 shows the evolution of the GSD by volume measured at different maximum vertical stress for samples with d_{50} = 0.50 mm. Between 0 and 5 MPa, an increase of the percentage of finer particle at constant d_{max} is observed. At 25 MPa the percentage of fines of the GSDs is further increased and all the GSDs converge for diameters d < 0.25 mm, while the upper part of the curves shows a slight rotation around d_{max}. This behaviour is related to a more pronounced increase of the fine particles for samples characterized by a lower initial uniformity. At 50 MPa a further increase of the percentage of fine smaller particles is measured, with the tail of the GSDs moves further upwards.

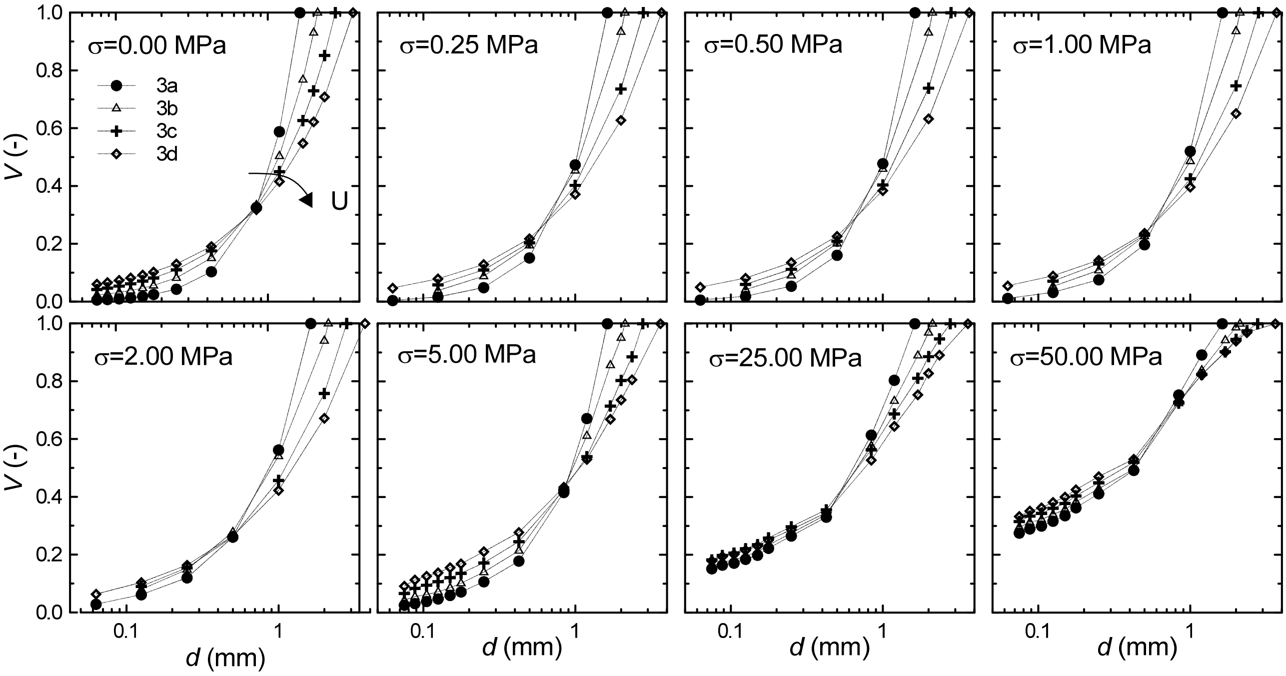

Figure 5. Grain size distribution by volume at increasing vertical stress for samples with d_{50}=1.00 mm

Figure 5 reports the evolution of the GSDs with loading for samples with d_{50}= 1.0 mm. Between 0 and 5 MPa the diameter of the intersection point d_{int} of the curves moves rightwards and upwards due to a small increase of the particles with d < 0.75 mm.

Figure 5 shows an overlapping of the tail of the GSD curves at 25 MPa for d < 0.425 mm, while the curves rotate around d_{max}. The percentage of particles with medium-small diameter increases between 5 and 25 MPa, especially for samples characterised by medium-low initial uniformity U.

Moving from 25 MPa to 50 MPa the upper parts of the GSDs tend to overlap with a counter clockwise rotation around the intersection point (V = 0.70 and d = 0.65 mm), and a slight reduction of the maximum diameter, somewhat more pronounced for higher uniformities. The fact that this was not observed for samples with an initial d_{50} = 0.5 mm, where the position of the intersection point was not changing with loading, is probably due to the higher strength of smaller particles which inhibits reductions of d_{max} and the associated increase of the percentage of medium sized particles.

The final GSDs, corresponding to a maximum vertical stress σ_{vmax} = 50 MPa, are very similar for all the samples tested (Figures 4 and 5), regardless of the initial values of U and d_{50}, particularly for the small diameters.

2. Modelling the GSD evolution with Weibull distribution

2.1 Weibull equation

The data illustrated above were fitted using a Weibull distribution. This is widely used in reliability engineering due its versatility and relative simplicity. The Weibull distribution is a flexible function used by different authors to describe the multi-scale features of granular materials with grain crushing (*e.g.* McDowell *et al.*, 1997; Zhang *et al.*, 2015; Zhang *et al.*, 2016).

The Weibull distribution is defined on positive and real numbers by the following repartition function:

$$F(X) = 1 - \exp[-(X/\lambda)^k] \tag{4}$$

where $F(X)$ is the cumulative probability that a variable is less or equal to X, $k > 0$ is a shape parameter and $\lambda > 0$ is a scale parameter of the distribution. The probability density function f is calculated from the derivative of the repartition function:

$$f(X) = k/\lambda^k \cdot X^{k-1} \cdot \exp[-(X/\lambda)^k] \tag{5}$$

Within the framework of statistic, particle breakage can be considered as a probabilistic event. When the stress or the strain has reached a sufficient level, some particles may break, depending on the contact forces applied on it and on its resistance. The breakage probability depends on:

- macroscopic factors, such as stress level, average diameter, coordination number which affect the particle contact force;
- microscopic factors, such as component minerals, particle shape, diameter and imperfections related to the particle resistance (Guida *et al*., 2016).

If X is the particle diameter, the Weibull distribution F represents the cumulative passing by volume. Figure 6 illustrates the effect of varying parameters k and λ on the shape of the GSD. The scale parameter λ represents the diameter at which V = 0.63. Fixing k and varying λ (Figure 6a) the Weibull distribution translates keeping its shape. The Weibull distribution is S-shaped with a maximum slope depending on the shape parameter k: as $k$increases, the distribution becomes steeper, while lower values of k result in a flatter shape of the distribution (Figure 6b). The derivative of F with respect to $\log(d)$:

$$\partial F/\partial \log(d) = d^{k-1}/\lambda^k \exp[-(d/\lambda)^k]\, \partial d/\partial \log(d) \tag{6}$$

has a characteristic "bell" shape attaining a the maximum proportional to the value of k through coefficient $k \cdot \ln(10)\,/e = 0.847\,k$ for $d = \lambda$ (Figs. 6c and 6d)

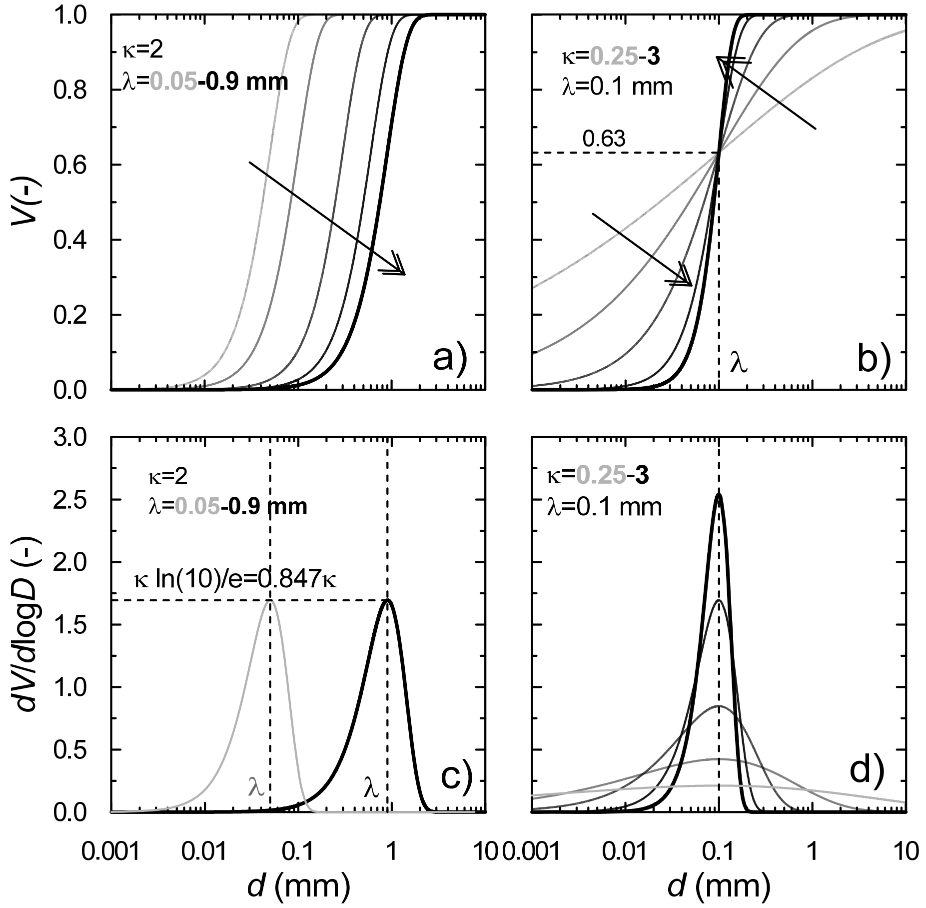

Figure 6 – Weibull distribution function for different values of λ (a) and $\boldsymbol{k}$ (b), and their derivatives by $\boldsymbol{log(d)}$ (c,d).

The experimental GSDs were described using a bimodal Weibull distribution, that better fits the grain size distribution than the single Weibull distribution function, due to the different evolution of larger and smaller particles as shown by the experimental results (Figures 7 and 8), weighted by w_1 and w_2 (where w_1+w_2=1):

$$V(d) = w_1 \cdot (1 - \exp[-(d/\lambda_1)^{k_1}]) + w_2 \cdot (1 - \exp[-(d/\lambda_2)^{k_2}]) \quad (7)$$

where V is the cumulative passing by volume, k_1 and k_2 the shape parameters, λ_1 and $\lambda_2$the scale parameters and d the diameter. The curve with weight w_1 and the curve with w_2=1-w_1 describe the GSD of larger particles and of smaller particles, respectively. The model parameters have been calibrated with the experimental results using the least square technique.

2.2 Interpretation of the results

Figure 7 (d_{50}=0.50 mm) and Figure 8 (d_{50}=1 mm) report the comparison between the data and their best fit through the bimodal Weibull distribution over the entire range of diameters, for the different uniformity and stress investigated.

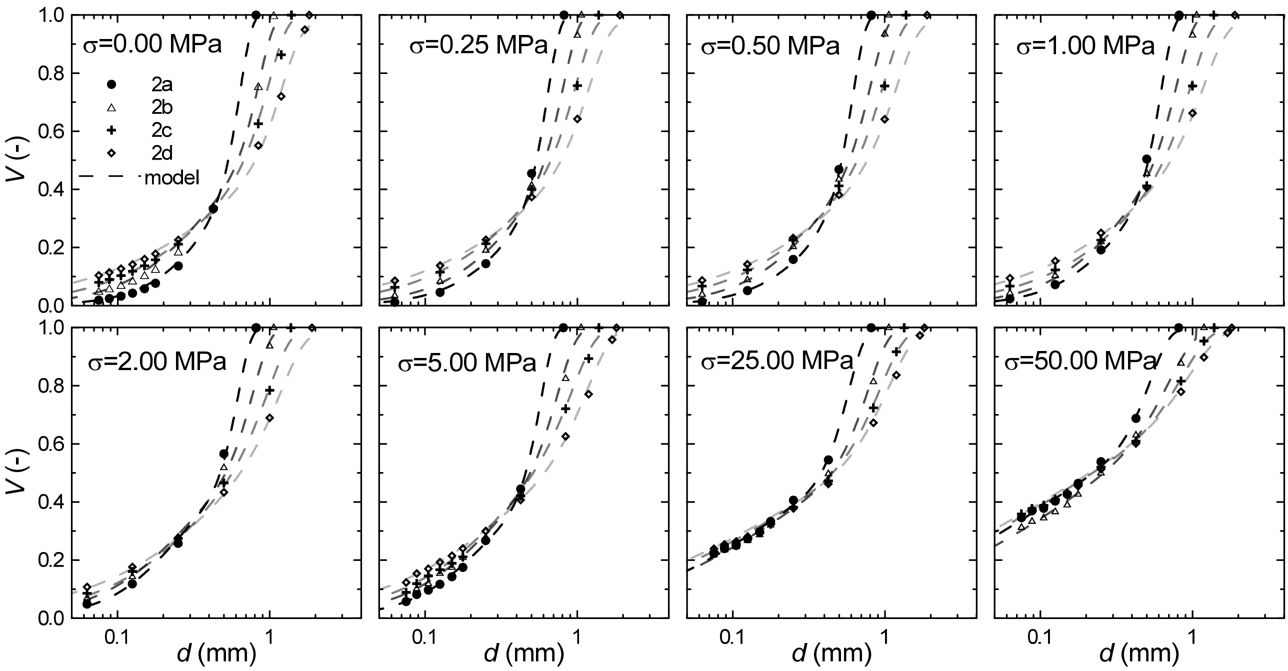

Figure 7. Comparison between model and experimental data with d_{50}=0.50 mm

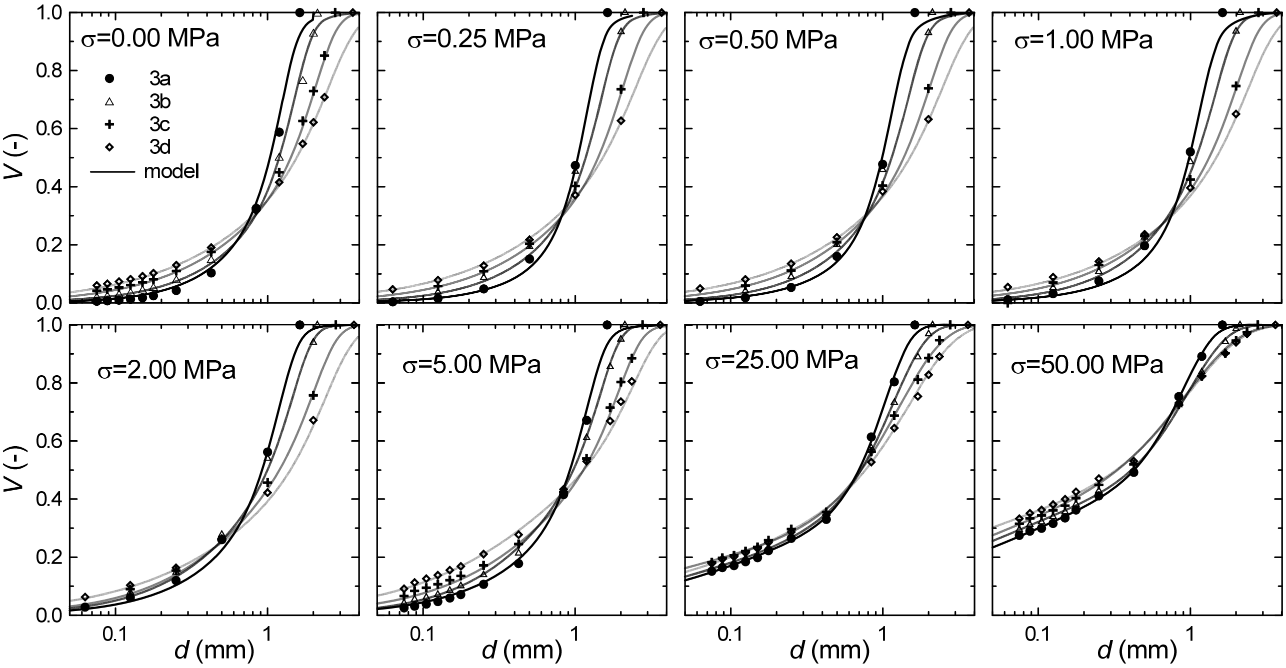

Figure 8. Comparison between model and experimental data with d_{50}=1.00 mm

Figure 9 shows the compressibility curves in the e-logσ_v plane for all the samples taken to a maximum vertical stress $\sigma_{v,max}$ = 50 MPa. The initial voids ratio of the samples characterised by d_{50} = 0.50 mm are quite scattered, especially the most and the less uniform grading, probably due to the different configuration that particles assume during sample preparation, that are not vibrated in order to not cause grain crushing or asperities breakage. However, even if they start from different values of the initial voids ratio, all the curves tend to converge for $\sigma_{v,max} \geq 10$ MPa, (Figs. 9a and b) and, therefore, the mechanical behaviour is unique.

The compressibility behaviour of a granular material with grain crushing is driven by two main mechanisms: particles rearrangement and grain crushing (including asperity breakage). Depending on the range of stress investigated, one or the other may prevail. The compressibility curve of LECA shows a typical S-shaped form. This can be divided in three ranges of vertical stress:

1) rearrangement of the particles in the form of sliding and rotation occurs with negligible grain crushing up to the initial crushing point stress σ_p;
2) most grain crushing occurs between the yielding point stress □p, corresponding to the stress of the big amount of crushing, and the stress corresponding to the point of inflection σ_s. In

this stress range the compressibility curve is steeper due to the particle crushing and rearrangement under medium-high stress;

3) for stress larger than that corresponding to the point of inflection, σ_s, particle crushing is no longer the main deformation mechanisms, even if some crushing still occurs, and the curve becomes flatter.

Figure 9 also reports the ranges of ~~crushing point~~ yielding stress and inflection point stress obtained from the experimental data. They are $\sigma_p = 0.5$ - 2 MPa and $\sigma_s = 6$-15 MPa with $d_{50} = 0.50$ mm and $\sigma_p = 0.7$-2.8 MPa and $\sigma_s = 7$ - 20 MPa with $d_{50} = 1$mm.

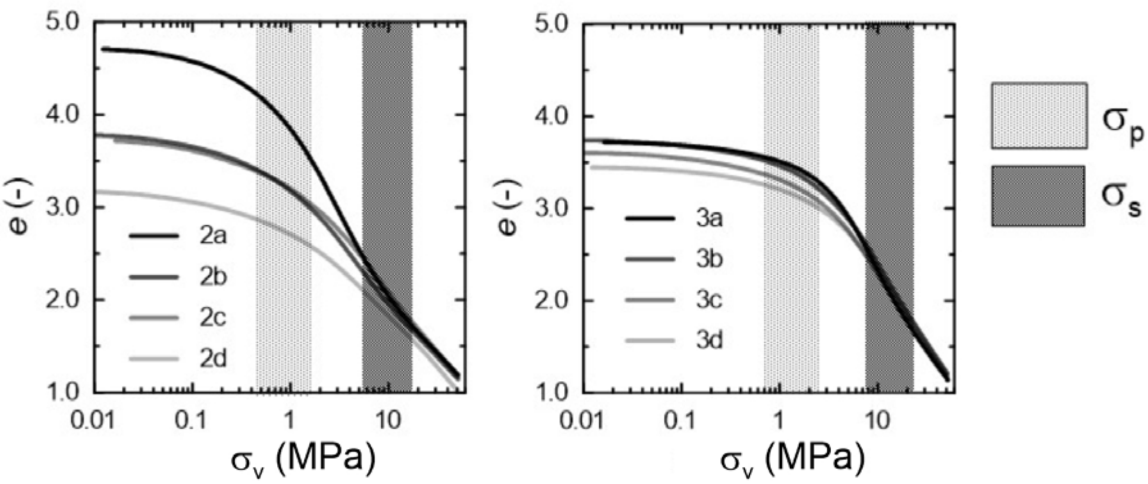

Figure 9. Compressibility curves in the logσ_v-e plane: a) d_{50}=0.50 mm; b) d_{50}= 1 mm.

Figure 10 shows the evolution of the fitting parameters $\lambda_1, k_1, \lambda_2,$ and k_2, obtained fitting the data with equation (7), as a function of the applied stress for all the samples with an initial $d_{50} = 0.5$ mm. As a first approximation, the evolution of the Weibull parameters may be taken as an indication of the evolution of grain crushing with applied stress. Parameters λ_1 and k_1, and λ_2 and k_2 represent the diameter at which the cumulative passing by volume is 0.63, and the maximum slope of the larger and smaller GSDs, respectively (see Figure 6).

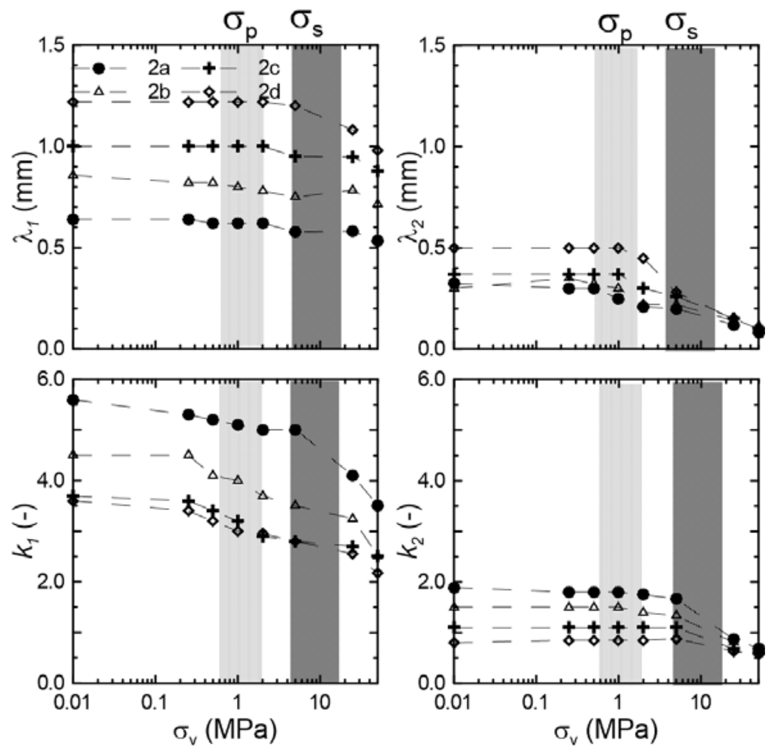

Figure 10. Weibull parameters for all samples with d_{50}=0.50 mm

Parameter λ_1 (macro diameters) exhibits a slightly decreasing trend for all the tested samples (Figure 10a) and an increasing slope in the range of stress corresponding to the inflection point; this is more pronounced for $U = 28$ (sample 2d). This shows that the larger particles start to break only as they cross the inflection stress. The macro GSD becomes flatter with increasing vertical stress, as k_1 decreases, with an increasing rate in the range of stress corresponding to the inflection point (Figure 10c).

For all the samples, parameter λ_2 starts to decrease well before parameter λ_1, at an applied vertical stress corresponding to the yielding point stress (Fig. 10b), with the implication that the smaller GSD shifts significantly to the left. The smaller GSDs become flatter as parameter k_2 decreases. As the stress approaches the range of σ_s, λ_2 decreases with a nearly linear rate in the semi-log plane. It is interesting that, at high stress, k_2 and λ_2 tend to unique values of $\lambda_2 \approx 0.10$ and $k_2 \approx 0.62$ independently of the initial uniformity U. This indicates that, upon loading, the GSDs of the smaller-diameters tend to become the same, irrespectively of their initial distribution. The data in Figure 10 suggest that the shape of the compressibility curve and the evolution of the GSD (represented by the evolution of λ and k) are linked to one another. As most crushing takes places at stresses between σ_p and σ_s, it is in this range that the compressibility curve is steepest, and this is particularly true for samples characterised by a lower initial uniformity (less graded). The compressibility curves overlap when the applied vertical stress is larger than the stress at the point of inflection and their slope after the point of inflection is the same independently of the initial voids ratio and uniformity.

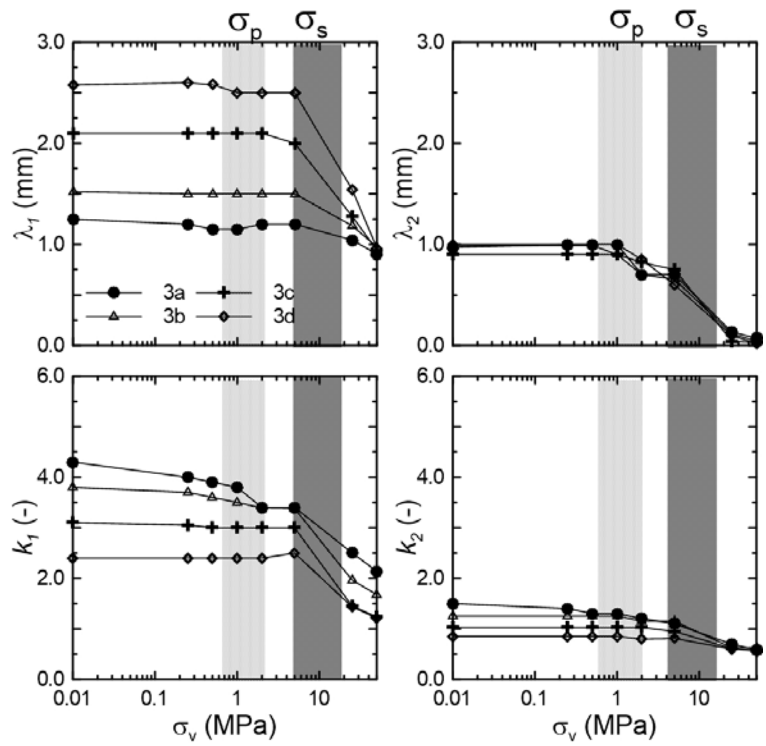

Figure 11. Weibull parameters for samples with d_{50}=1.00 mm

Figure 11 shows the evolution of Weibull parameters for all the samples with an initial d_{50} = 1 mm. λ_1 and k_1 (larger diameters) are essentially constant up to stresses in the range between σ_p and σ_s, and then start to decrease, possibly with the only exception of sample characterised by an initial U = 3.5. At the maximum applied vertical stress, λ_1 takes a unique value of $\lambda_1 \approx 0.95$, and this is reflected in the fact that, at 50 MPa, the GSD of samples with an initial d_{50} = 1.0 mm, tend to overlap (see Fig. 5). Parameter λ_2 (Fig. 11b) shows a drastic reduction, starting at stress levels in the range of the crushing point stress, indicating a substantial shift to the left of the GSD associated to the micro-diameters. Parameter k_2 shows a decrease with applied stress after the crushing point stress, σ_p, indicating that as the GSD associated to the smaller-diameters shifts to the left, it also becomes flatter. For samples with initial $d_{50} = 1.0$ mm, at large vertical stress, parameters λ_2 and k_2 tend to unique values of $\lambda_2 \approx 0.05$ and $k_2 \approx 0.60$. The tendency of the parameters k_2 and λ_2 to become the same independently by the initial GSD is consistent with the existence of an ultimate GSD, anyway further crushing of the larger diameter is expected in order to describe the ultimate GSD with a unique fractal curve. The value of w_2 for the tested samples at higher vertical stress ranging between 0.4 (GSD with initial d_{50}=0.5 mm) to 0.6 (GSD with initial d_{50}=1.0 mm).

Conclusions

The paper reports the results of an extensive laboratory investigation of grain crushing under one-dimensional compression, conducted on an artificial material with crushable grains. The samples were prepared by dry pluviation, in reduced diameter cells in order to reach higher stresses. The long-term objective of the study is to gain a deeper understanding of the behaviour of granular materials with crushable grains from moderate to high stress, and to develop constitutive equations that incorporate the effects of an evolving grain size distribution.

The material used for the experimental work is a Light Expanded Clay Aggregate (LECA) whose grains break at relatively low stress. Reconstituted samples were prepared with different initial grain size distributions and their evolution observed under one-dimensional compression. The grain size distributions before and after loading were described using a bimodal Weibull function, resulting from the superposition of two curves with weights w_1 (referred to the upper part of the grain size curve, bigger diameter) and w_2=1-w_1 (referred to the lower part of the grain size curve, smaller diameter). The evolution of the best-fit Weibull parameters with applied stress carries information on the mechanisms of grain crushing and can be linked to the compressibility of the material.

The observed compressibility curves show a typical S-shape characterized by two point of changing of slope, yielding stress point and the stress at the point of inflection respectively, dividing the investigated stress range into three regions. For stresses lower than the yielding stress, particle rearrangement occurs in the form of sliding and rotation. For stresses between the yielding stress and the stress corresponding to the point of inflection, significant particle crushing superimposes to particle rearrangement, causing a marked increase of compressibility. For stresses larger than the stress corresponding to the point of inflection, particle crushing is no longer the main deformation mechanism, and, although some breakage still occurs, the compressibility decreases.

This is demonstrated by the evolution of the best-fit Weibull parameters. Specifically, the best-fit parameters describing the micro diameters start to decrease as the applied vertical stress reaches the yielding point stress, while larger stresses are required to modify the parameters describing the macro diameters, which start decreasing at the stress corresponding to the inflection point stress.

References

ALONSO E., TAPIAS M., GILI J. (2012) - *Scale effects in rockfill behaviour*. Géotechnique Lett. **2**, 3, pp. 155–160

BANDINI V., BIONDI G., CASCONE E., DI FILIPPO G. (2016) - *Dynamic image analysis of*

Etna Sand in one-dimensional compression. Measurement in press

CASINI F., VIGGIANI G.M., SPRINGMAN S.M. (2013) - *Breakage of an artificial crushable material under loading*. Granular Matter **15**, 5, pp. 661-673.

DI PRISCO C., BUSCARNERA G. (2010) -Progettazione, esecuzione e controllo di rilevati leggeri realizzati in argilla espansa. Rivista Italiana di Geotecnica, 3, pp. 10-29.

EINAV I. (2007) - *Breakage mechanics. Part 1: theory*. Journal of the Mechanics and Physics of Solids, **55**, 6, pp. 1274–1297

GUIDA G., BARTOLI M., CASINI F., VIGGIANI G.M.B. (2016) - *Weibull Distribution to Describe Grading Evolution of Materials with Crushable Grains*. Procedia Engineering, 158, pp. 75-80.

HARDIN B.O. (1985) - Crushing of soil particles. *Journal of Geotechnical Engineering*, ASCE 111, 10, pp. 1177–1192.

LACKENBY J., INDRARATNA B., MCDOWELL G., CHRISTIE D. (2007) - *Effect of confining pressure on ballast degradation and deformation under cyclic triaxial loading*. Géotechnique **57**, 6, pp. 527–536

LADE P.V., YAMAMURO J.A., BOPP P.A. (1996) - Significance of particle crushing in granular materials. *Journal of Geotechnical Engineering* ASCE 122 (4): 309–316.

LEE, K. L., & FARHOOMAND, I. (1967). *Compressibility and crushing of granular soil in anisotropic triaxial compression*. Canadian geotechnical journal, 4(1), 68-86.

LOBO-GUERRERO, S., & VALLEJO, L. E. (2005). *Discrete element method evaluation of granular crushing under direct shear test conditions.* Journal of Geotechnical and Geoenvironmental Engineering, 131(10), 1295-1300.

LUZZANI L., COOP M. R. (2002) - *On the relationship between particle breakage and the critical state of sands*. Soils Found. **42**, 2, pp. 71–82.

MARKS B., EINAV I. (2015) - A mixture of crushing and segregation: The complexity of grainsize in natural granular flows. *Geophys. Res. Lett.*, 42, pp. 1-8.

MCDOWELL G.R., BOLTON M.D., ROBERTSON D. (1996) - *The fractal crushing of granular materials*. Journal of Mechanics and Physics of Solids **44**, 12, pp. 2079–2102.

NAKATA A.F.L., HYDE M., HYODO H. (1999) - *A probabilistic approach to sand particle crushing in the triaxial test*. Géotechnique **49**, 5, pp. 567–583.

NAKATA Y., HYODO M., HYDE A.F., KATO Y., MURATA H. (2001) - *Microscopic particle crushing of sand subjected to high pressure one-dimensional compression*. Soils Found. **41**, 1, pp.69–82

OKADA, Y., SASSA, K., & FUKUOKA, H. (2004). *Excess pore pressure and grain crushing of sands by means of undrained and naturally drained ring-shear tests*. Engineering geology, 75(3), 325-343.

OVALLE C., FROSSARD E., DANO C., HU W., MAIOLINO S., HICHER P.Y. (2014) - The effect of size on the strength of coarse rock aggregates and large rockfill samples through experimental data. *Acta Mechanica* **225**, 8, pp. 2199–2216.

SAMMIS C.G., BEN-ZION Y. (2008) - *Mechanics of grain-size reduction in fault zones*. Journal of Geophysical Research, 113, B02306, pp. 1-12.

SIMONINI P. (1996) - *Analysis of behaviour of sand surrounding pile tips*. Journal of Geotech. Engineering, 122, pp. 897-905.

WOOD D.M., MAEDA. (2008) - *Changing grading of soil: effect on critical states*. Acta Geotechnica, **3**, pp. 3–14

YASUFUKU N., HYDE A.F.L. (1995) - *Pile end bearing capacity in crushable sand*. Géotechnique 45, 4, pp. 663–676.

ZHANG C., NGUYEN G., EINAV I. (2012). *The end-bearing capacity of piles penetrating into crushable soils*. Géotechnique 63, 5, pp. 341–354.

ZHANG, X., ZHANG, H., & WEN, Z. (2015). *Axial crushing of tapered circular tubes with graded thickness.* International Journal of Mechanical Sciences, 92, 12-23.

ZHANG, Y. D., BUSCARNERA, G., & EINAV, I. (2016). *Grain size dependence of yielding in granular soils interpreted using fracture mechanics, breakage mechanics and Weibull statistics.* Géotechnique, 66(2), 149-160.
ZICCARELLI M. (2016) - *Evolution of Grain-size Distribution of Pumice Sands in 1-D Compression*. Procedia Engineering, **158**, pp. 27-32.

List of Tables

Table 1. Samples tested

identifier	$d_{50,P}$ **[mm]**	U_P **[-]**	$d_{50,V}$ **[mm]**	U_V **[-]**	$\sigma_{v,max}$ **[MPa]**							
					0.25	0.5	1.0	2.0	5.0	12.6	25	50
2a	0.5	3.5	0.5	2.9	●	●	●	●	●	●	●	●
2b	0.5	7.0	0.6	4.3	●	●	●	●	●	●	●	●
2c	0.5	14	0.7	6.7	●	●	●	●	●	●	●	●
2d	0.5	28	0.8	8.7	●	●	●	●	●	●	●	●
3a	1	3.5	1.1	2.9	●	●	●	●	●	●	●	●
3b	1	7.0	1.2	4.4	●	●	●	●	●	●	●	●
3c	1	14	1.3	6.7	●	●	●	●	●	●	●	●
3d	1	28	1.5	9.2	●	●	●	●	●	●	●	●